Investigating the collapsar model using simulation

Candidate number 24514
Department of Physics, University of Bath, Bath BA2 7AY, United Kingdom

Abstract. The collapsar model predicts that long gamma-ray bursts (LGRBs) require a metallicity of less than 0.3 $Z_{\odot}$, but they have been observed from host galaxies that are mostly above this limit. This discrepancy means there is potentially a big lack in our understanding of how gamma-ray bursts (GRBs) are formed, and how much they depend on metallicity and star formation rate. Observations are mostly galaxy-integrated measurements, as we cannot currently measure the local metallicity of gamma-ray bursts, so the aim of this research was to use simulation to see if theory and observation contradict or not. This was achieved, as a model was found for selecting galaxies as GRB host galaxies, which had parameters that agreed with the collapsar model, while also producing results comparable with observation. This is because the model preferentially chose galaxies with more metal-poor regions but produced distributions of more metal-rich host galaxies, as seen in observation. This suggests GRBs can occur in low-metallicity regions of high-metallicity galaxies, meaning the collapsar model is still valid.

1. Introduction

Gamma-ray bursts (GRBs) are the most luminous explosions in the Universe; they are divided into two classes, short and long, with long gamma-ray bursts (LGRBs) having a duration longer than 2 seconds and these will be the focus of this report. They are associated with the core collapse of massive stars into accreting black holes, so they are good tracers of star formation at high redshift [1]; they were thought to be unbiased tracers until theory suggested a metallicity bias [2]. Their afterglows also have such a high luminosity, that they can illuminate their host galaxies. This makes it possible to probe these distant galaxies for information about their interstellar medium, such as chemical and dust content, and the evolution of the galaxy [3].

Rotating Wolf-Rayet stars (hot and massive stars) that have lost their outer hydrogen, were theorised as the progenitors of GRBs in 1993 [2]. Now known as the collapsar model, it predicted that the iron core collapses to form a black hole, with the excess material around the core forming an accretion disk due to the angular momentum of the star. Neutrino energy is then deposited along the rotation axis, exciting matter to extremely high temperatures and velocities, causing the matter to escape the black hole along the rotation axis in the form of relativistic jets.

This model was improved upon in 1999, with the progenitor star having a mass of 25-35 $M_{\odot}$ [4]. There was also a requirement for low metallicity because wind-driven mass loss is thought to be proportional to the square root of the metallicity [5], so there is less mass loss at lower metallicities. This is because the winds are driven by the interactions of photons with the absorption lines in the metals in the stellar atmosphere. These winds become stronger at higher metallicities because the presence of more metals means there are more absorbing lines, and a higher probability of interaction [6]. Winds are required to remove the hydrogen envelope, so the jets can escape, but if too much mass is lost then angular momentum is lost as well. Angular momentum is needed to form the accretion disk that feeds the jets. A low metallicity maintains the angular momentum and is therefore required for GRBs to occur [4]. More specifically, GRBs are only possible up to a metallicity of 0.3 $Z_{\odot}$ [5], above which there is not enough angular momentum for the process to take place.

The GRB prompt emission is then caused by internal shocks within the relativistic jet, as the plasma moving at different velocities collides with itself [4]. An afterglow of lower frequency, produced when the front of the jet collides with interstellar medium, was also predicted in 1993 [7], and observed in 1997 when GRB 970228 also had an associated X-ray afterglow [8].

One important event was the detection of GRB 980425, which was the closest GRB ever detected, at a redshift of $z = 0.0085$. Also, an afterglow was not observed, instead a supernova, SN 1998bw. Even though GRBs are usually brighter than supernovae, the GRB transient looked like a SN because the light from the SN was brighter and drowned out the GRB light. This was thought to be very atypical and therefore not enough to verify that GRBs are associated with SNe [9]. However, the collapsar model did predict that all GRBs of this type will also have an associated supernova, like SN 1998bw [4]. This prediction was confirmed in 2003, when the detection of the very luminous GRB030329 was followed by SN 2003dh [10], as supernovae are generally not observed until the GRB has faded. This confirmed that normal LGRBs are linked to SNe, and therefore the death of a massive star.

The main current problem with the collapsar model now, is the metallicity limit of 30% solar metallicity mentioned previously. Most GRBs are billions of light years away, and the spatial resolution of current equipment is not high enough to measure the metallicity of stars, so it is measured from the gas in their host galaxies. Gas-phase metallicity is measured using the ratios of emission lines in star-forming H II regions, as these emission lines are mostly excited by massive stars [11]. The oxygen abundance is commonly used along with units $12 + \log(O/H)$, where O/H is the ratio of the number densities of oxygen and hydrogen. This gives a logarithmic scale of metallicity, with no negative values. This gas-phase metallicity can be assumed to be equal to the metallicity of the massive stars, since they are young and are likely to have formed out of gas of the same metallicity [11].

Originally, many studies suggested that GRBs indeed prefer low-metallicity environments [12], until the Swift mission showed that a lot of GRBs occurred in regions highly obscured by dust. These are known as dark GRBs: events where the optical afterglow is not detected or is much fainter than expected considering the X-ray afterglow [13]. This is because dust extinction and neutral hydrogen absorption supresses optical light but not X-ray light. No optical afterglow will prevent the host galaxy from being found and therefore excluded from samples; these selection effects with bias against dusty galaxies led to the wrong conclusions about metallicities of host galaxies [13].

With a more complete sample, it became apparent that more GRBs occurred in metal-rich galaxies than previously thought. Data from a more recent study [14] showed that about 90% of host galaxies in the sample had a metallicity greater than the theorised limit of $0.3\ Z_{\odot}$ (equal to roughly 8.1 in units of $12 + \log(O/H)$). This varies between studies due to different samples and different diagnostics used to measure the metallicity. Observation seems to contradict with theory, and this raises the question of whether the collapsar model is incorrect or GRBs just occur in metal-poor regions of metal-rich galaxies. This is what this report will be investigating.

As said before, observational techniques are limited and cannot definitively test this aspect of the model, so this report will show the use of simulation to test the hypothesis that LGRBs with metal-rich host galaxies are just occurring in metal-poor regions of them. Section 2 of this report will introduce the cosmological model used for this investigation: IllustrisTNG. Section 3 will describe the method used for selecting LGRB host galaxies and how the necessary data was retrieved. In section 4 we showcase the optimal model that was found to select host galaxies similar to those that are observed, and the predictions of this model. In section 5 we will discuss any faults or concerns with this model or IllustrisTNG, along with concluding what the results mean for the collapsar model.

2. Simulation

The requirements for the simulation being used for this research were a large volume, for a high number of galaxies, and a good spatial resolution, for obtaining the metallicity of the local regions where LGRBs would originate. Therefore, the best option was to use IllustrisTNG, which is a set of state-of-the-art hydrodynamical cosmological simulations. It is very accessible, and has a big volume with a reasonable resolution, making it the top candidate for this project. For the full timeline of the universe, from redshift $z = 127$ to $z = 0$, the simulations realistically follow the evolution of galaxies, including the dark matter, gas, stellar and black hole components [15].

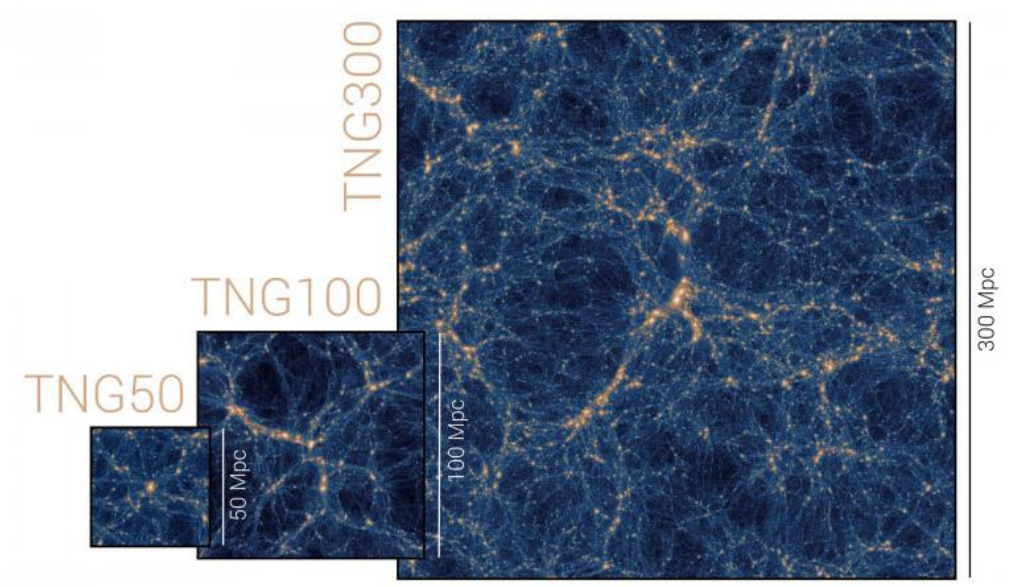

Figure 1. Size comparison of the three different simulation volumes in IllustrisTNG. TNG50 has the smallest side-length and volume but the highest resolution, making it most suitable for this investigation. Figure reproduced from [15].

In IllustrisTNG, the stars are formed from dense gas, where star particles record their birth time and are given the metallicity of the interstellar medium (ISM) from which they were born. Star particles age according to stellar lifetime tables, and aging stellar populations return gas and metal mass to the ISM according to yield tables for different types of stars. Mass is returned by being spread amongst the 64 nearest gas cells. The metals are then transported with the fluid flow, leading to the metal enrichment of the ISM [16].

There are three different simulation volumes in IllustrisTNG: TNG50, TNG100, and TNG300, with the number referring to the length of one side of the simulation's cubic volume, in comoving Mpc. This is demonstrated in figure 1, where the illustration of IllustrisTNG has a filamentary structure comparable to that observed in our Universe; this encapsulates the detail and accuracy of the simulation and why it was chosen. For example, TNG50 has side-length of 50 Mpc and thus the smallest volume, but a mass resolution one hundred times greater than TNG300, making it useful for the investigation of small-scale processes. This resolution is why TNG50 was utilised for the research detailed in this report [17], although even TNG50 can only resolve regions hosting thousands of stars.

There are four resolution levels for TNG50 with TNG50-1 having the highest resolution (2×2160^3 resolution elements) and was therefore the best choice. Four selected TNG runs and their physical properties are shown in table 1. TNG50-1 has the smallest particle masses, and therefore the highest mass resolution, which is why it was chosen for this research.

The data is organised into one hundred snapshots at different redshifts. Each snapshot has a set of attributes (such as redshift and the number of each type of particle), and a catalogue of subhalos, or galaxies, and halos, or galaxy clusters. Each subhalo has a long list of attributes, including an associated star formation rate (SFR), mass and metallicity. The mass is divided between all the components: dark matter, gas, stars, and black holes, while the metallicity is divided into stellar and gas components. This

Table 1. Properties of four selected TNG simulations. The parameters are box side-length, initial number of gas cells (equal to the initial number of dark matter cells), and the target baryon and dark matter particle masses. TNG50-1 has the smallest particle mass, and hence the greatest mass resolution.

Run	L_{box} [cMpc / h]	$N_{GAS,DM}$	m_{baryon} [10^6 $M_\odot$]	m_{DM} [10^6 $M_\odot$]
TNG50-1	35	2160^3	0.08	0.45
TNG50-2	35	1080^3	0.68	3.63
TNG100-1	75	1820^3	1.4	7.5
TNG300-1	205	2500^3	11	59

information is also present at the particle-level. As only the gas-phase metallicity can be measured at high redshift, only that will be of interest. Its values are given by $Z = M_{Z,gas}/M_{gas}$, the fraction of gas-mass composed of metals. These were converted to units of 12+log(O/H) for comparisons with observational values.

3. Methods

The objective was to obtain the necessary data from TNG, using a model to select galaxies likely to be GRB hosts, and analyse the data to compare with observations. As explained in the previous section, the TNG50-1 simulation was used for its high resolution, making it the best option, even if it is still not close to being able to resolve singular GRBs events. Out of the hundred available snapshots, snapshot 33 (at redshift $z \sim 2$), was chosen for it being the most common redshift for observed LGRBs [18].

Distributions of the stellar masses and star formation rates of GRB host galaxies were used to filter out the majority of subhalos in the snapshot. No GRBs have been observed from galaxies with stellar mass $< 10^7$ $M_\odot$ or SFR < 0.5 $M_\odot$ yr^{-1} [1], so we do not want to include any low-mass or low-SFR (passive) galaxies in the data for this investigation. With low-mass and low-SFR galaxies being very dim in the sky, this could be a selection effect, but the aim is to reproduce observations, so this will be ignored. The high-mass and star-forming galaxies that we are interested in, the viable galaxies, are in a particular region in the stellar mass-SFR parameter space, which is shown in figure 2. On top of the scatter plot of viable subhalos is the best-fit line, which was derived empirically from a sample from the MOSDEF survey [19]. This highlights one problem with Illustris TNG: the star formation main sequence is different to that which is observed at the same redshift. At a stellar mass of 10^9 $M_\odot$, a difference of about 0.6 dex is seen. This was likely to be an issue due to the trivial dependence of GRB emissions on SFR.

In each of the remaining subhalos, the cells' coordinates were converted to polar, and then the cells were filtered to only keep those within ten stellar half-mass radii (R_e) from the galaxy centre (point with the lowest gravitational potential energy). This was done because the area within 10 R_e encapsulates more than any galaxy, but makes sure to cut out any distant, passive populations of stars where GRBs would be unlikely to occur. These cells were then filtered further to only keep star-forming cells (SFR > 0), before being copied onto a new array. Here, all cells with gas-phase metallicity Z greater than the variable Z_{max} (initial value of 0.3 $Z_\odot$) were removed. The ratio of the length of these two arrays, or the

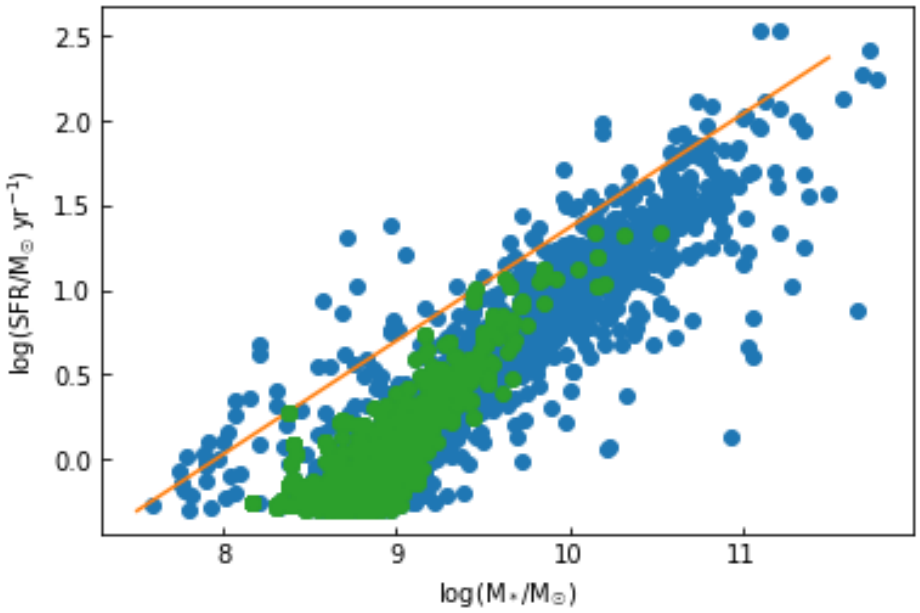

Figure 2. Relation between stellar mass and star formation rate. Blue points show all viable subhalos (above stellar mass and SFR threshold) in the $z = 2$ snapshot. Green points show the sample of 1000 randomly selected subhalos, according to the optimal model described in the next section. The orange line is the best-fit line derived empirically from the $z \sim 2.3$ sample from the MOSDEF survey [19].

fraction of star-forming gas cells with metallicity $Z < Z_{max}$, F, was calculated, along with the sum of the SFR array, the total star formation rate in these low-metallicity gas cells, T. The product of these values was used as the weighting for the random selection of 1000 subhalos as GRB hosts. This is because the collapsar model predicts that LGRBs favour a lower metallicity, so galaxies with lots of metal-poor, star-forming gas cells are more likely to be GRB hosts. The metallicities, star formation rates and stellar masses of this subhalo sample were plotted as cumulative distribution functions (CDFs) to be compared with observation.

4. Results

Each model that was used had three key values that defined them: the metallicity limit, Z_{max}, and the exponents of F and T. Therefore, the weights used for random selection were given by

$$W = F(Z_{max})^m T(Z_{max})^s \quad (1)$$

with m and s being the two other key values to be defined in the model. The initial model used had $m = s = 1$, and $Z_{max} = 0.3$. Cumulative distribution functions were plotted to compare the properties of the sample of randomly selected subhalos with all the viable subhalos (stellar mass > 10^7 $M_\odot$ and SFR > 0.5 $M_\odot$ yr^{-1}) in the snapshot. A K-S test was carried out, which determines the statistical difference between them by comparing the two distributions and giving the largest difference between the functions across all x-values (D-statistic) and the probability that the two samples are from the same distribution (p-value). This was done as the observations [1] that we were comparing to has the results of K-S tests from comparing the properties of LGRB host galaxies and the larger sample of star-forming galaxies. We used this to test the accuracy of our model for selecting samples of LGRB-like host galaxies. This is because we cannot trust absolute values from observations; this is most relevant for metallicity given the uncertainty with metallicity diagnostics, which will be discussed later. Therefore, comparing the relative differences between the simulated LGRB hosts and the rest of the star-forming galaxy population was a more accurate way of testing the model.

The D-statistics and p-values that were produced from the initial model are shown in table 2, along with those calculated from observation. The CDFs were also compared with the observational results shown in figure 3 [1]. For the initial model, the metallicity distributions looked similar in shape, but

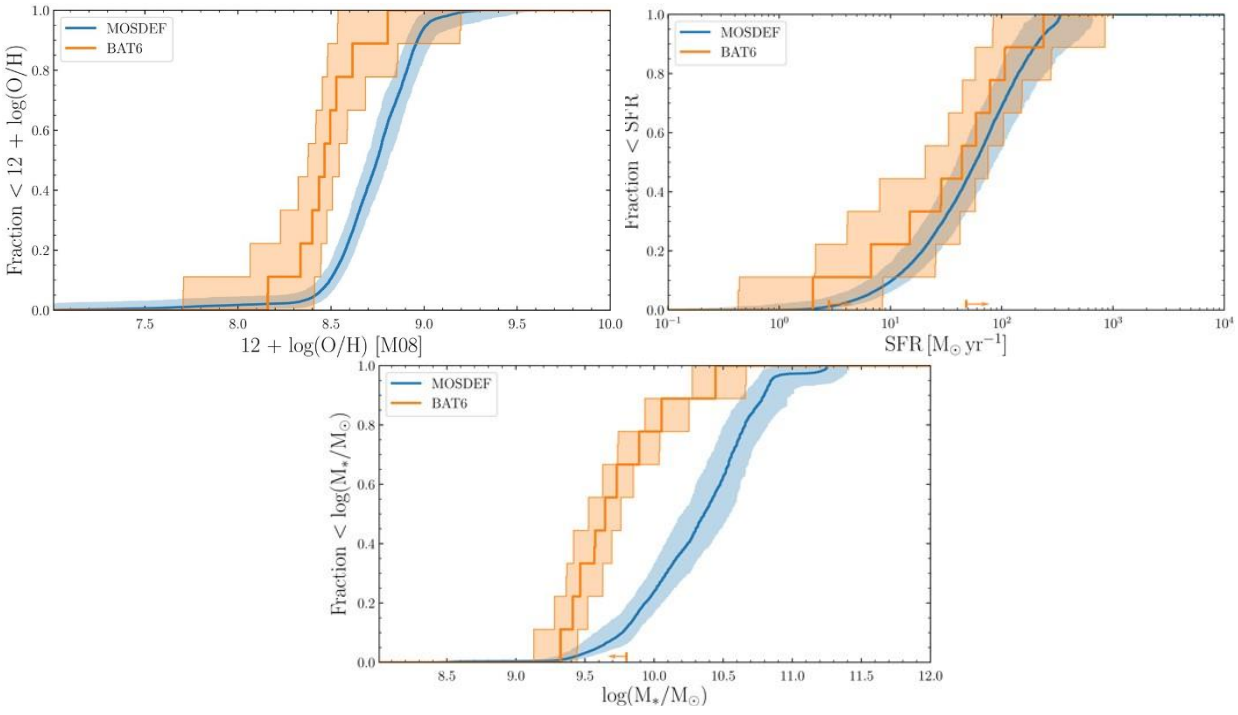

Figure 3. Three cumulative distribution function plots for the observed metallicity, SFR and stellar mass of GRB host galaxy sample, BAT6, along with a larger galaxy sample at the same redshift, MOSDEF. Figures reproduced from [1].

Table 2. K-S test values produced from using three models for selecting GRB hosts in TNG. The first row contains the values calculated from observations of GRB hosts [1]. The initial model had the parameters, $m = s = 1$, and $Z_{max} = 0.3$. The second model had the parameter values, $m = 1$, $s = 2$, and $Z_{max} = 0.5$ The optimal model had the parameter values, $m = 2.5$, $s = 0$, and $Z_{max} = 0.3$.

	Metallicity		SFR		Stellar mass	
	D-statistic	p-value	D-statistic	p-value	D-statistic	p-value
Palmerio (2019)	0.67	6.31×10^{-4}	0.37	0.316	0.63	2.51×10^{-3}
Initial model	0.219	5.44×10^{-30}	0.102	9.03×10^{-7}	0.0987	2.25×10^{-6}
Larger *s*	0.148	8.87×10^{-14}	0.536	7.97×10^{-188}	0.465	1.51×10^{-138}
Optimal model	0.389	1.16×10^{-95}	0.295	2.10×10^{-54}	0.324	1.59×10^{-65}

the SFR and stellar mass distributions, which are shown in figure 4a, were too close to the distribution of the whole population, and the wrong shape. This meant the D-statistics were much smaller than what was found in observation.

As GRBs are good tracers of star formation, the SFR weighting was increased ($s = 2$) and the metallicity limit was also changed ($Z_{max} = 0.5$). It led to the sample having too many high-mass and metal-rich host galaxies, due to SFR being positively related to stellar mass and metallicity. This produced a sample with metallicity too similar to the valid subhalo population and a greater SFR and stellar mass than the whole population, very different to what is seen in figure 3. The CDFs for the SFR and stellar mass are shown in figure 4b for comparison with the initial model, and the values from the K-S tests for this model are also in table 2. For this model, the D-statistics were much closer to matching observation for SFR and stellar mass. However, this was because each of the pairs of distributions were further apart, but the wrong side of each other. In figure 3 the GRB sample is to the left of the MOSDEF

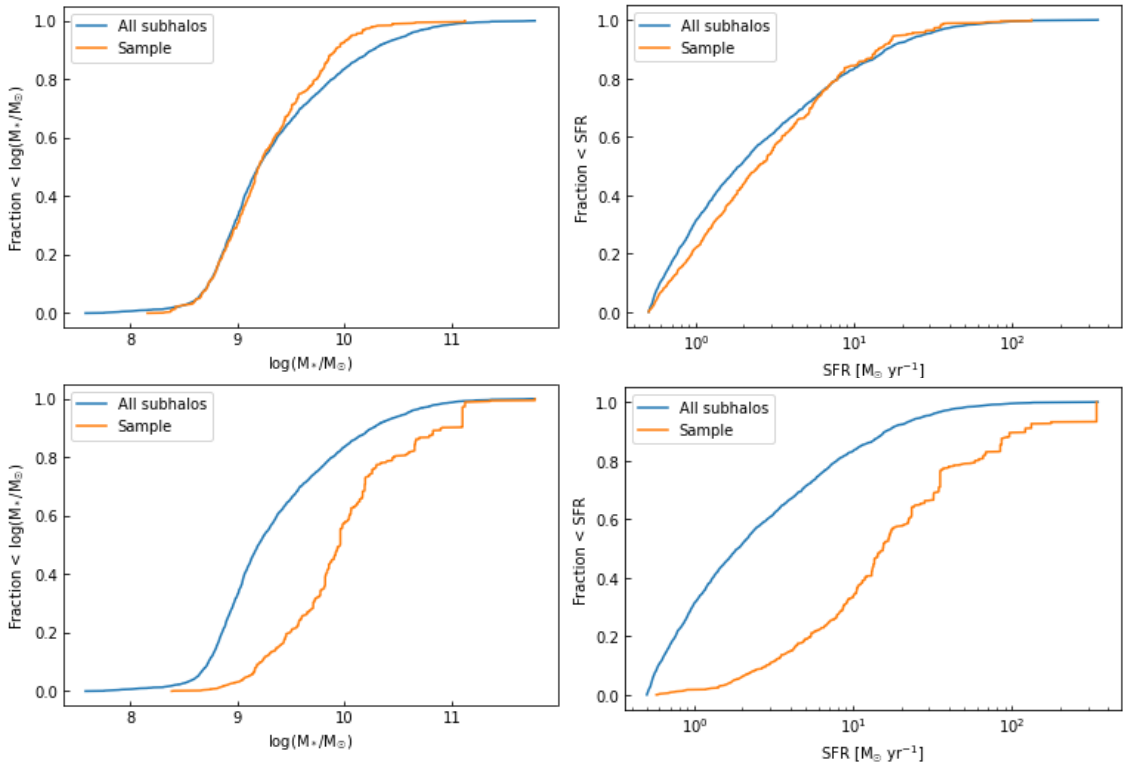

Figure 4. *Top*: (4a) Cumulative distribution function plots for the stellar mass and SFR of subhalos in IllustrisTNG. The orange line is plotted from the random selection of 1000 subhalos, using the model with parameters: $m = s = 1$, and $Z_{max} = 0.3$. The blue line is the plot of the whole population of all viable subhalos. *Bottom*: (4b) Same properties plotted as for the top, but with the model with parameters: $m = 1$, $s = 2$, and $Z_{max} = 0.5$.

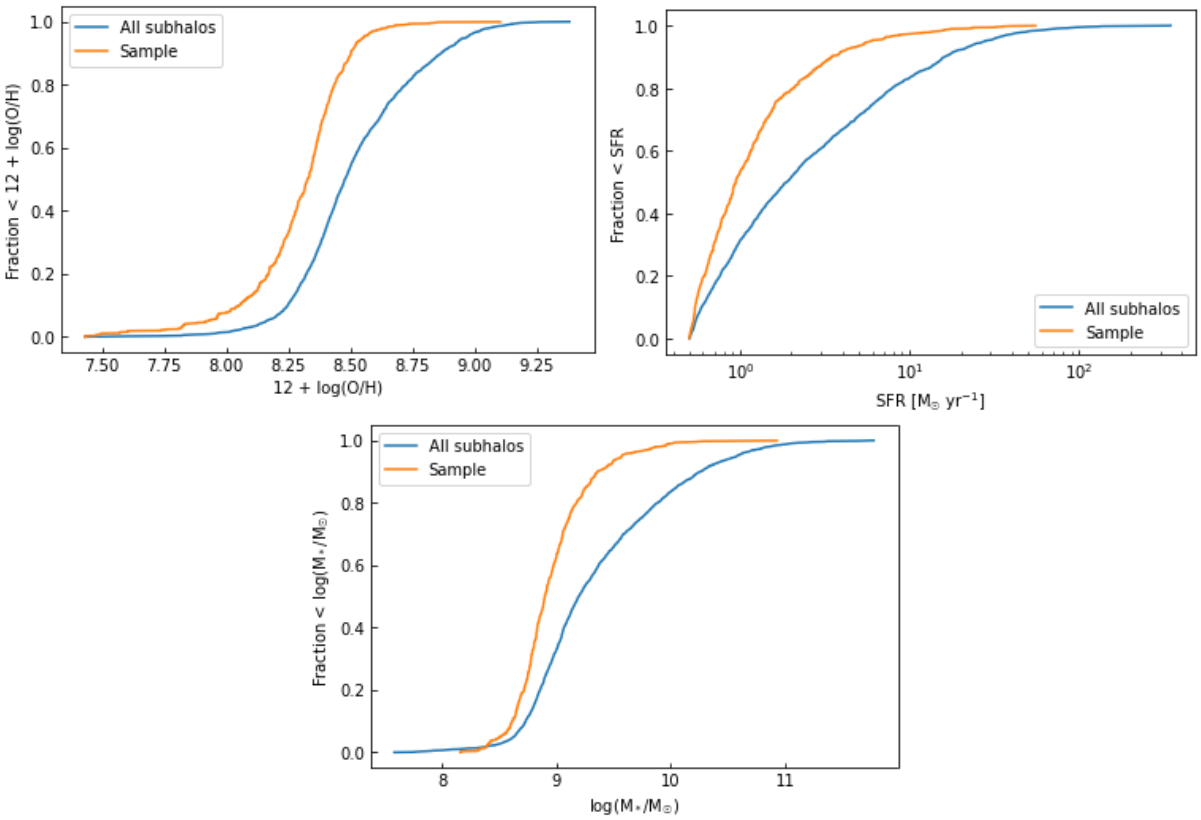

Figure 5. Cumulative distribution function plots for the metallicity, SFR and stellar mass of subhalos in IllustrisTNG, with the orange line being a random selection of 1000 subhalos, with a large weighting on the fraction of cells with low Z. The model used had parameters: m = 2.5, s = 0, and Z_{max} = 0.3. The blue line is plotted from the larger population of all viable subhalos. Each plot matches the observation quite well, except for SFR.

sample for each property, but in figure 4b, the randomly selected sample is to the right of the sample of all viable subhalos.

To correct this, the SFR weighting s was reduced, and the fraction weighting m was increased, because the collapsar model predicts the necessity for low-metallicity environments. These were adjusted until the CDFs matched observation the most: the shapes were similar, and the D-statistics were as close to those in table 2 as possible. This came in the form of m = 2.5, s = 0, and Z_{max} = 0.3. This refined model produced D-statistics much closer to that of observation, and these are shown in table 2. The p-values for all models are far lower than those calculated from observation because there is no uncertainty in the data obtained from the TNG simulation. The CDFs that were produced are shown in figure 5 and predicted a median metallicity of 8.3, SFR of 0.9 $M_\odot$ yr^{-1}, and stellar mass of $10^{8.9}$ $M_\odot$. This compares to the data in figure 3, which gave an average metallicity of 8.45, SFR of 40 $M_\odot$ yr^{-1}, and stellar mass of $10^{9.6}$ $M_\odot$, although absolute values of metallicity should be treated with some skepticism. There is a significant difference between the SFR values, but this can be partially attributed to the systematic difference between SFR values in TNG and observation, as shown in figure 2.

4.1. Particle analysis

Once we found a model optimal for selecting subhalos that reflected the LGRB host galaxies that are observed, we then explored the particle-level properties of the randomly selected sample, to see what the model predicted. From this sample of a thousand selected galaxies, 1 cell with $Z < 0.3$ $Z_\odot$ was randomly selected per galaxy (with linear cell-SFR weighting) as the local regions to host a LGRB. More cumulative distribution functions were then plotted for the radial offset of the cell from its centre (in units of stellar half-mass radii), and the cell metallicity and SFR to see what the model predicted. The metallicity and SFR were normalised by dividing them by the maximum value for that subhalo.

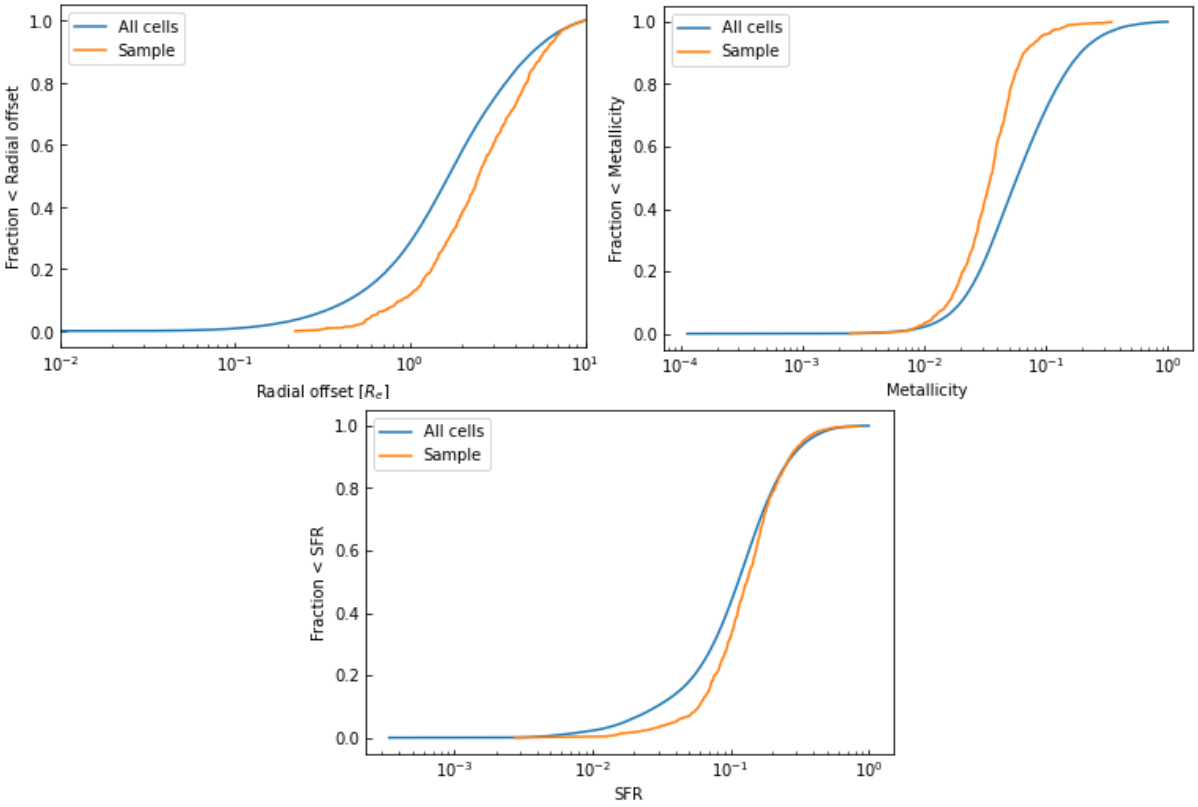

Figure 6. Three cumulative distribution function plots of the radial offset, metallicity and SFR of cells within the 1000 selected subhalos. The sample is one low-*Z* cell chosen per subhalo, with the selection weighted by SFR, so this explains the shift of the orange line from the blue in the two right-side plots. The top-left plot suggests a median radial offset of 2-3 R_e for GRBs.

These CDFs were plotted along with distributions of all the star-forming cells in all of the selected subhalos and are shown in figure 6. Due to the limitations of observation of GRBs, there is not a wealth of observational data to compare these distributions to, only the radial offset of the GRB has any, although limited, data [20]. Figure 6 shows that, compared to the general population of star-forming cells, LGRBs have a lower metallicity and higher SFR, although these are both by construction, due to the sample containing only low metallicity cells and being selected with a SFR weighting. The median radial offset of the GRBs was between 2 and 3 R_e, with them being predicted to be further from the centre than the general population. This is a product of the low metallicity requirement, with metallicity decreasing radially, as has been observed with metallicity gradients [21]. Observational data for the radial offset of GRBs in their host galaxies is displayed in figure 7. Here, the average radial distance from the galaxy centre for a GRB to occur is shown to be 0.59 R_e which is much lower than found in figure 6.

Any further plots needed for analysis could be produced from the data retrieved using the above methods. For example, figure 8 shows plots relating subhalo and cell properties. There were a large number of points plotted on top of each other, so they were converted to number density plots, allowing the highest density regions of the plot to be more visible. The centre of the yellow area predicts that most GRBs occur at a subhalo SFR of 1 $M_\odot$ yr^{-1}, and a metallicity of roughly 8.35; the normalised cell SFR (divided by the maximum value in the subhalo) was 0.13 and the normalised metallicity was 0.03. The most important conclusion from figure 8, is that the average subhalo metallicity was comparable to observation, while the metallicity of the cell containing the GRB was much lower than the rest of the cells in its galaxy, which is consistent with the predictions of the collapsar model. This solidifies the idea of GRBs occurring in metal-poor regions of metal-rich galaxies.

5. Discussion

The optimal model had a high weighting on the fraction of cells with low *Z*, showing GRBs care more about being in metal-poor environments than the SFR, which matches the predictions of the collapsar

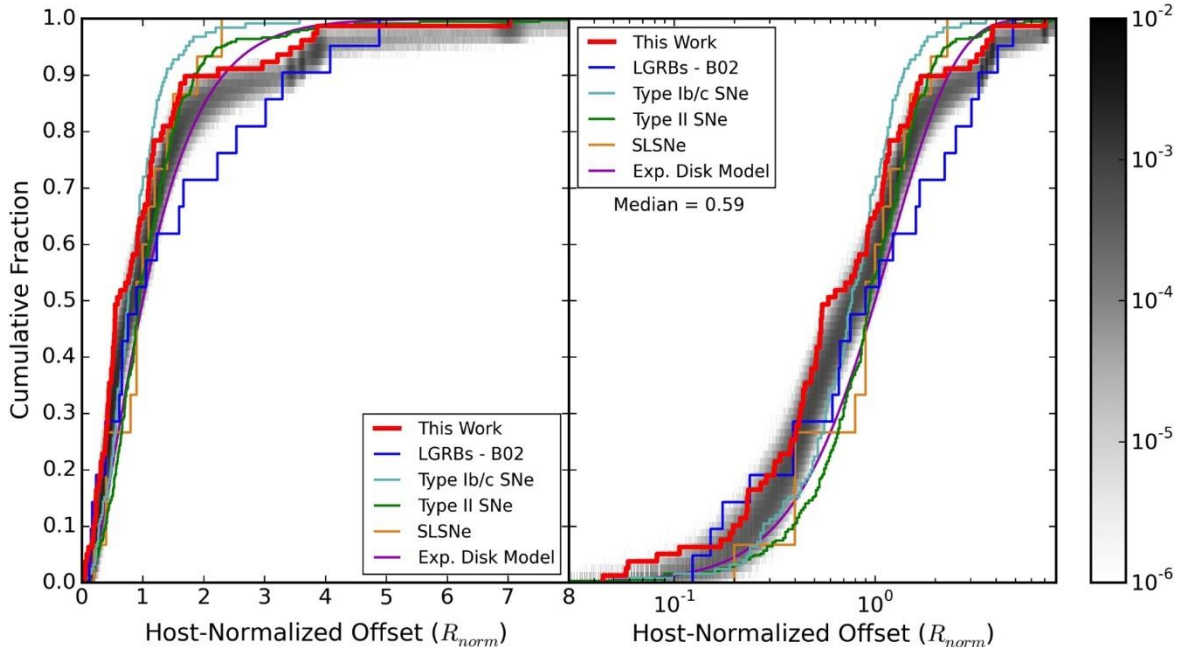

Figure 7. Cumulative distributions of the radial offset of GRBs within their host galaxies. Left-side plot has a linear-scale on the x-axis, right-side has a log-scale. Figure reproduced from [20], where the article's sample is shown by the red line.

model, with the 0.3 $Z_{\odot}$ metallicity limit. Although this model has $s = 0$, there is still some SFR selection bias, with the original filtering of the subhalos only including SFR > 0.5 $M_{\odot}$ yr^{-1}.

It was chosen as the best model due it being the closest to matching observation. Any comparisons with absolute metallicity measurements should only be considered skeptically, as there is a lot of uncertainty in the measurements of galaxy metallicity. This is because typical techniques for determining gas-phase metallicity are based on theoretical or empirical calibrations, so any inaccuracies in these calibrations spoil the reliability of the measurements [22]. This is why the relative differences between the samples were compared instead.

When comparing the SFR distributions in figure 3 and figure 5, it is visible that there is a significant difference in the SFR values, with observations having much higher values. Absolute values in observation can be inaccurate but this difference could be the fault of TNG. Figure 2 shows the systematic difference in SFR values between TNG and observation. At the median stellar mass found in figure 5, the SFR in TNG galaxies is about 0.6 dex lower than what is observed; this accounts for a significant fraction of the ~ 1.4 dex difference seen between the samples. This has also been investigated

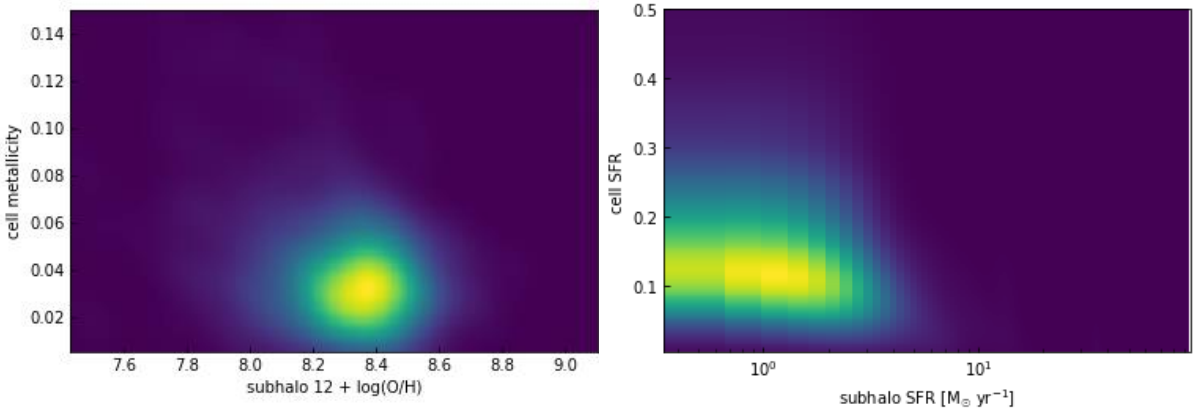

Figure 8. Two number density plots for the relation between subhalo and cell metallicity and SFR. The y-axes are the cell property, normalised by dividing by the maximum value in that subhalo. The x-axes are the subhalo property. The left-side plot suggests GRBs occur in metal-poor regions of their host galaxies.

previously and was speculated to be the result of the foundational limitations of theoretical models but could also be due to the contamination from non-star-forming sources inflating the measured values of the SFR [23].

When comparing radial offset distributions in figure 6 and figure 7, the predicted average (between 2 and 3 R_e), is much larger than is observed (0.59 R_e). However, radial offset measurements require spatially resolving the local region of GRB prompt emission, which is easier at low redshift but becomes more difficult at high redshift, where most GRBs occur. This creates a lot of uncertainty in the measurements, meaning this difference should not be considered significant. Furthermore, there is a difference in the normalisation used for the IllustrisTNG data and the observational data. The effective radius R_e is given by the stellar half-mass radius in TNG, but the observed R_e is calculated as the half-light radius (radius that contains half of the light from a galaxy). It is a good approximation for the stellar half-mass radius but any dust obscuring light from stars will affect the value that is measured and could be a reason for the differences seen between our results and observational data.

Another potential reason for this difference is that, in IllustrisTNG, particles at lower R_e are too metal rich to be selected by our model as LGRB host regions. This would mean that, if the observations are reliable, then they would be implying that GRBs do occur in metal-rich environments, opposing the collapsar model. However, this would have to be verified with more sensitive observations.

6. Conclusions

This investigation succeeded in helping verify the collapsar model, because the model that produced results most consistent with observation of GRB hosts, required a high weighting in the fraction of star-forming gas cells within a subhalo, that have metallicity less than 0.3 $Z_\odot$. This matches a key idea of the collapsar model, which predicts that a low metallicity (specifically $Z < 0.3\ Z_\odot$) is required to maintain the angular momentum that is needed for GRBs to occur. It was also shown that GRBs likely occur in metal-poor regions of more metal-rich galaxies, while there was little discrepancy between the observed values of galaxies' metallicities and the values found in TNG.

Future work in this area would include finetuning the model further and applying it to potential future Illustris simulations. Also, the accuracy of measuring metallicities could be improved; for example, the JWST could help improve the calibrations used for high redshift galaxies. Other technological advancements could also help improve the spatial resolution of the spectroscopic measurements, and potentially show empirically that GRBs are produced in metal-poor regions of galaxies with a higher metallicity.

Acknowledgements

I would like to give many thanks to my project supervisor, Dr Patricia Schady, for making this work possible. Her knowledge, guidance and advice were invaluable to this project. I would also like to thank my project partner Luke Hamill-Smith, for help with some of the coding aspects of this research and for double-checking results.

References

[1] Palmerio JT, et al. Are long gamma-ray bursts biased tracers of star formation? Clues from the host galaxies of the Swift/BAT6 complete sample of bright LGRBs. *Astron Astrophys*. 2019 Mar;**623**(A26):1-18.

[2] Woosley SE. Gamma-Ray Bursts from Stellar Mass Accretion Disks around Black Holes. *Astrophys J*. 1993 Mar 1;**405**(1):273-7.

[3] Campana S, Salvaterra R, Tagliaferri G, Kouveliotou C, Grindlay J. Probing the very high redshift Universe with gamma-ray bursts: prospects for observations with future X-ray instruments. *Mon Not R Astron Soc*. 2011 Jan 6;**410**(3):1611-6.

[4] MacFayden AI, Woosley SE. Collapsars: Gamma-Ray Bursts and Explosions in "Failed Supernovae". *Astrophys J*. 1999 Oct 10;**524**(1):262-89.

[5] Woosley SE, Heger A. Progenitor Stars of Gamma-Ray Bursts. *Astrophys J*. 2006 Feb 1;**637**(2):914-21.

[6] Hainich R, Shenar T, Sander A, Hamann W-R, Todt H. The metallicity dependence of WR winds. *Proc Int Astron Union*. 2016 Nov;**12**(S329):171-5.
[7] Paczynski B, Rhoads JE. Radio Transients from Gamma-Ray Bursters. *Astrophys J*. 1993 Nov;**418**(1):L5-L8.
[8] Wijers RAMJ, Rees MJ, Meszaros P. Shocked by GRB 970228: the afterglow of a cosmological fireball. *Mon Not R Astron Soc*. 1997 Jul;**288**(4):L51-L56.
[9] Galama TJ, et al. Discovery of the peculiar supernova 1998bw in the error box of GRB980425. *Nature*. 1998 Oct 15;**395**(1):670-2.
[10] Hjorth J, et al. A very energetic supernova associated with the γ-ray burst of 29 March 2003. *Nature*. 2003 Jun;**423**(6942):847-50.
[11] Wang E, Lilly SJ. Gas-phase Metallicity as a Diagnostic of the Drivers of Star Formation on Different Spatial Scales. *Astrophys J*. 2021 Apr 5;**910**(137):1-33.
[12] Le Floc'h E, et al. Are the hosts of gamma-ray bursts sub-luminous and blue galaxies? *Astron Astrophys*. 2003 Mar 3;**400**(2):499-510.
[13] Perley DA, et al. The Host Galaxies of Swift Dark Gamma-ray Bursts: Observational Constraints on Highly Obscured and Very High Redshift GRBs. *Astron J*. 2009 Dec;**138**(6):1690-708.
[14] Kruhler T, et al. GRB hosts through cosmic time. VLT/X-Shooter emission-line spectroscopy of 96 γ-ray-burst-selected galaxies at $0.1 < z < 3.6$. *Astron Astrophys*. 2015 Sep;**581**(A125):1-32.
[15] Nelson D, et al. The IllustrisTNG Simulations: Public Data Release. *Comput Astrophys Cosmol*. 2019 May 14;**6**(2):1-29.
[16] Torrey P, et al. The evolution of the mass-metallicity relation and its scatter in IllustrisTNG. *Mon Not R Astron Soc*. 2019 Jan 23;**484**(4):5587-607.
[17] Nelson D, Pillepich A, Springel V, Pakmor R, Weinberger R, Genel S, Torrey P, Vogelsberger M, Marinacci F, Hernquist L. First Results from the TNG50 Simulation: Galactic outflows driven by supernovae and black hole feedback. *Mon Not R Astron Soc*. 2019 Aug 29;**490**(3):3234-61.
Pillepich A, et al. First Results from the TNG50 Simulation: the evolution of stellar and gaseous discs across cosmic time. *Mon Not R Astron Soc*. 2019 Sep 9;**490**(3):3196-233.
[18] Le T, Mehta V. Revisiting the Redshift Distribution of Gamma-Ray Bursts In the Swift Era. *Astrophys J*. 2017 Mar 1;**837**(17):1-12.
[19] Sanders RL, et al. The MOSDEF Survey: A Stellar Mass-SFR-Metallicity Relation Exists at $z \sim 2.3$. *Astrophys J*. 2018 May 10;**858**(99):1-18.
[20] Blanchard PK, Berger E, Fong W. The Offset and Host Light Distributions of Long Gamma-Ray Bursts: A New View from HST Observations of Swift Bursts. *Astrophys J*. 2016 Feb 1;**817**(144):1-30.
[21] Sanchez-Menguiano L, Sanchez SF, Perez I, Ruiz-Lara T, Galbany L, Anderson JP, Kruhler T, Kuncarayakti H, Lyman JD. The shape of oxygen abundance profiles explored with MUSE: evidence for widespread deviations from single gradients. *Astron Astrophys*. 2018 Jan;**609**(A119):1-47.
[22] Sommariva V, Mannucci F, Cresci G, Maiolino R, Macroni A, Nagao T, Baroni A, Grazian A. Stellar metallicity of star-forming galaxies at $z \sim 3$. *Astron Astrophys*. 2012 Mar 6;**539**(A136):1-12.
[23] Donnari M, Pillepich A, Nelson D, Vogelsberger M, Genel S, Weinberger R, Marinacci F, Springel V, Hernquist L. The star formation activity of IllustrisTNG galaxies: main sequence UVJ diagram, quenched fractions, and systematics. *Mon Not R Astron Soc*. 2019 Mar 12;**485**(4):4817-40.